Structure of Liquid Iron at Pressures up to 58 GPa

Guoyin Shen,[1,*] Vitali B. Prakapenka,[1] Mark L. Rivers,[1,2] and Stephen R. Sutton[1,2]
[1]*Consortium for Advanced Radiation Sources, University of Chicago, Chicago, Illinois 60637, USA*
[2]*Department of Geophysical Sciences, University of Chicago, Chicago, Illinois 60637, USA*
(Received 12 August 2003; published 4 May 2004)

We report structural data on liquid iron at pressures up to 58 GPa measured by x-ray scattering in a laser heated diamond anvil cell. The determined structure factor preserves essentially the same shape along the melting curve. Our data demonstrate that liquid iron at high pressures is a close-packed hard-sphere liquid. The results place important constraints on the thermodynamic and transport properties of liquid iron and the melting curve of iron.

DOI: 10.1103/PhysRevLett.92.185701 PACS numbers: 64.70.Dv, 07.35.+k, 61.10.Nz, 61.20.Qg

The properties of iron at high pressure are of great interest because it is a classic transition element and is a dominant component in terrestrial planet cores. Many studies have revealed information about the state of crystalline iron and provided insight into the nature of planetary cores [1]. While the high pressure behavior of crystalline iron has been extensively investigated, experimental studies on liquid iron are few and have been limited to pressures below 5 GPa [2,3]. This imbalance is apparently not due to the lack of scientific importance of liquid iron, but rather to the experimental difficulties arising from the extreme conditions required to melt iron at relevant pressure. In fact, liquid iron is of significant importance in geophysics. Recent solar tidal evidence [4] indicates that the Martian core could be entirely liquid. Earth's liquid outer core accounts for about 96% of the core by volume. Dynamo action in the fluid outer core is responsible for sustaining Earth's magnetic field [5] and the dynamics of this process are largely related to thermodynamic and transport properties of the outer core liquid. Knowledge of the local, atomic structure of liquid iron and its pressure dependence provides a crucial ingredient in understanding these properties.

In this letter, we present the results of structure measurements on liquid iron up to 58 GPa, which was made possible by the combination of a third generation synchrotron and an optimized laser heated diamond anvil cell (DAC). Our results provide a structural basis for understanding the origin of thermodynamic and transport properties of liquid iron, and place tight experimental constraints of the melting curve of iron, with the latter based on x-ray diffraction/scattering signals from crystalline and liquid phases at high pressure. Iron is one of a few systems that has been extensively studied theoretically with various models [6–9]. The new experimental results represent important tests of these theoretical predictions for advancing our understanding of dense liquid metals in general. The developed experimental technique involves measuring weak x-ray scattering from liquids at *in situ* high pressures and high temperatures, which should be applicable to other studies that require *in situ* measurements, such as phase transitions and thermal equations of state.

Experiments were performed at the GeoSoilEnviroCARS at the Advanced Photon Source. The iron sample was loaded in a DAC and heated under high pressure using a double-sided laser heating system [10]. The diamond anvil culet size was 500 μm in diameter. A hole of 200 μm in diameter was drilled at the center of a preindented stainless steel gasket to 30 μm. Iron powder (99.9 + % purity, Alfa) was pressed into a disc to a thickness of ~10 μm, from which a flake of ~50 μm in diameter was loaded in the gasket hole with two dry NaCl layers (~ 10 μm thick) sandwiched as a pressure medium as well as thermal insulating layers. NaCl is chosen for its low shear and bulk moduli, simple x-ray diffraction pattern, high x-ray luminescence, and higher melting temperatures than iron at pressures over ~30 GPa [11]. The entire loading was in a glove box in an argon atmosphere to avoid any moisture. Cubic boron nitride seats were used in the DAC for its hardness and x-ray transparency, resulting in a large opening angle for x-ray scattering. The x-ray position was closely monitored by the x-ray luminescence signal arising from the NaCl layers and was aligned to the laser heating area where temperatures were measured. The collection time for x-ray scattering was 10 s. The experimental pressure-temperature conditions are shown in Fig. 1 together with a previously determined phase diagram of iron [12]. At each pressure, *in situ* x-ray diffraction/scattering patterns were acquired as temperature was increased, until clear diffuse scattering from the liquid was observed. Therefore, the obtained structural data for liquid iron represent experimental conditions near and above the melting curve of iron (Fig. 1). Temperature was determined from thermal radiation spectra fitted to the Planck radiation law [10]. Pressure was determined at room temperature from x-ray diffraction patterns using the equation of state of NaCl [13]. After initial heating, pressure differences before and after laser heating were found to be within 1 GPa. At high temperature, thermal pressure effect needs to be taken into account [14], which

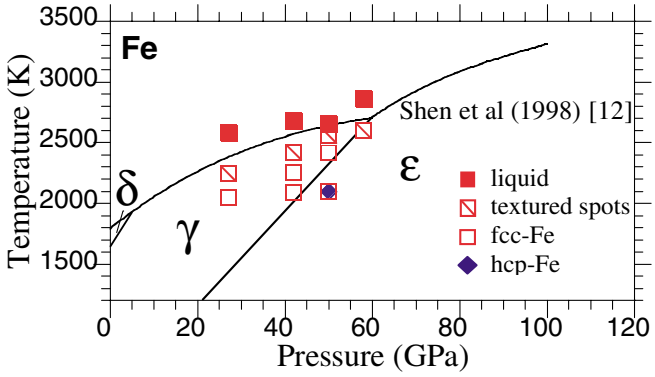

FIG. 1 (color online). Experimental conditions of the current study together with a phase diagram of iron 12. Error bars in temperature are from multiple measurements. Errors in pressure represent uncertainties from measurements before and after heating and are less than the symbol size (see text for a discussion of thermal pressure contribution).

in principle could be experimentally estimated by mixing with a standard material whose equation of state is known. An experimental study [15] shows that, for samples that had been through several previous heating cycles at the same spot on the sample, the pressure-temperature path can be interpreted within the constant pressure-constant volume continuum. This path should depend on individual sample configuration, with softer media and larger heating spot being closer to the constant pressure situation. In this study, in order to avoid any chemical reaction at extremely high temperatures above melting, no other material was mixed with the iron sample. The region probed with the x-ray beam had been laser heated several times before reaching the molten state. Considering the use of a soft medium material (NaCl), the molten state of the sample, and the large laser heating spot size (~ 20 μm, compared to the x-ray beam size of <10 μm), the pressure change at high temperature in our case should be less than that previously observed (5–10 GPa) [15,16].

Figure 2 shows the measured x-ray diffraction/scattering patterns at 50 GPa. At a temperature of 2420 ± 40 K, crystalline diffraction from fcc phase (γ-Fe) is clearly observed [Fig. 2(a)]. After increasing temperature to 2540 ± 55 K, only a few diffraction spots from γ-Fe [Fig. 2(b)] can be seen. These spots show textured features different from those at room temperature and at high temperatures far below melting. The origin of these textured spots is still under investigation. The integrated pattern [Fig. 2(d)] shows that the background at 2540 K is almost identical to that of crystalline phase at 2420 K. We interpret the point at 2540 K to be still in the crystalline state and, therefore, below melting. At all other pressures in this study, we find that the intensities of textured spots are weak and spot numbers range from none to just a few. This leads to the conclusion that disappearance of diffraction is not a reliable criterion for determining melting. Upon further increasing of temperature to

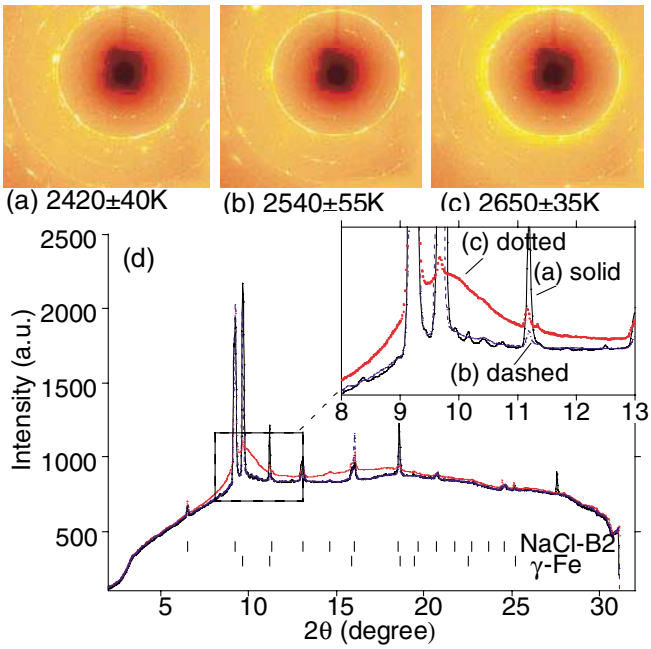

FIG. 2 (color online). X-ray diffraction/scattering patterns at 50 ± 1 GPa. (a), (b), and (c) are x-ray diffraction/scattering images recorded at different temperatures; (d) integrated patterns corresponding to these images: (a) solid line, (b) dashed line, and (c) dotted line. An insert is shown around the major diffuse band region. Clear diffuse scattering from liquid iron is observed at 2650 ± 35 K. The crystalline phase below melting was found to be γ-Fe. Other crystalline diffraction lines arise from the pressure medium (NaCl-B2).

2650 ± 35 K, a complete diffuse ring is observed, reflecting the liquid state of iron at this pressure [Fig. 2(c)]. The positive measure of a liquid state allows bracketing melting point. The diffuse scattering signals from the liquid are also used for structural determinations.

Since the x-ray radiation traverses diamond anvils, medium and sample, accurate background subtraction is crucial. The diffraction pattern just below melting was used as a reference for subtracting the incoherent and the background scattering [17]. The obtained coherent scattering was normalized by applying the Krogh-Moe-Norman method [18]. An optimization procedure was further applied for an improved structure factor [19]. The derived structure factors are shown in Fig. 3(a). As can be seen, the shape of the structure factors at high pressures is similar to that at ambient pressure. The compression effect is mainly reflected by peak shifts to larger Q values in structure factors.

The structure of liquid transition metals can be generally interpreted as a simple fluid in which the arrangement of atoms is similar to the hard-sphere model. The hard-sphere structure factor using the Percus-Yevick equation [20] is given by the function of the packing fraction $\eta = \pi\rho\sigma^3/6$, where ρ is the average number density of atoms and σ the hard-sphere diameter. If we

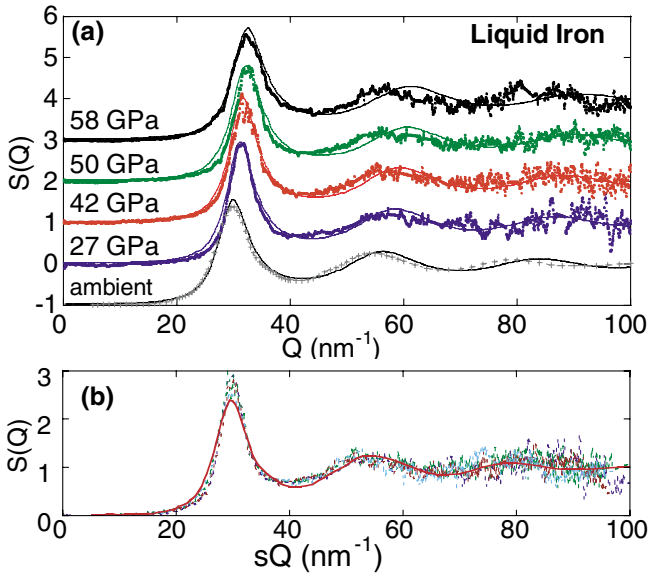

FIG. 3 (color online). (a) Structure factors of liquid iron determined by x-ray scattering at high pressures. Solid lines are hard-sphere structure factors using the Percus-Yevick equation, with η being 0.43–0.44. Vertical scales are offset for clarity. Data at ambient pressure are from Ref. [3]. (b) Structure factors plotted as a function of the scaled momentum transfer (see text for definition). The scaled patterns show that the structure factor remains the same shape at pressure-temperature conditions nearly along the melting curve. The structure factor at ambient pressure [3] (solid line) is shown for comparison.

employ the hard-sphere model [20], the results in Fig. 3(a) can be explained by keeping the packing fraction essentially constant with pressure and decreasing the hard-sphere diameter with increasing pressure. Thus for liquid iron, the hard-sphere model provides a basic reference for describing the liquid, although improvement in the large Q region may be made by introducing more sophisticated perturbation theories [21].

Generally speaking, the compression behavior of liquids is related to the nature of structure and bonding. The increase of the coordination number and packing fraction [22], or even liquid-liquid transitions [23], has been observed in both liquids and glasses with open structures and anisotropic bonding. For liquid metals with close-packed structures and isotropic metallic bonding, changes of local atomic configuration are generally not seen with pressure. Our data show that liquid iron at high pressure is consistent with the general characteristics of close-packed liquid metals.

First principle molecular dynamics simulations [8,9] also predict that liquid iron is a close-packed liquid under outer core conditions. Simulations show that the structure factor as a function of scaled momentum transfer sQ is constant along the melting curve [7], where Q is the momentum transfer, and the factor s is defined by $Q_0(1)/Q_p(1)$, with $Q_0(1)$, $Q_p(1)$ the positions of the first peak in structure factors at ambient pressure and high pressures, respectively. Plotting our data with the scaled momentum transfer [Fig. 3(b)] does show that the structure factor retains the same shape at pressure-temperature conditions nearly along the melting curve. The success of simple scaling indicates that there is no structural change of liquid iron in the covered pressure-temperature range. The structure measured at the highest pressure (58 GPa) is similar to that at ambient pressure. Speculation on structural changes at high pressure can be ruled out. This conclusion does not agree with the result from a study at pressures below 5 GPa using a large volume press [2] where liquid iron indicated structural changes near the δ-γ-1 triple point.

The structure of liquid iron at high pressure should provide insights on macroscopic properties such as viscosity, one of the key geophysical parameters needed for modeling the geodynamo. Our results of liquid iron remaining a hard-sphere liquid over a wide pressure range help justify extrapolation to high pressures of the viscosity data of liquid iron at relatively low pressures [24] and provide structural verifications of theoretical predictions [8]. Contrary to a large enhancement in the viscosity of liquid iron by 5–12 orders of magnitude from ambient to core pressures [25], our data support the view that the viscosity of liquid iron does not change significantly along the melting curve and is close to the value at ambient pressure (~ 6 cP).

By assuming an invariant structure for liquid iron along the melting curve, Stevenson [26] derived a melting relation that can be reduced to Lindemann's law in the classical high temperature harmonic approximation. Our results for liquid iron provide experimental evidence for the invariant structure, and thus for the validity of Lindemann's law. For iron, this law should be regarded as an appropriate method for extrapolating the melting curve [1,27].

The structural data can also be used to interpret the seismic parameter Φ, one of the important observable parameters in seismology defined by $\Phi = V_P^2 - \frac{4}{3}V_S^2$, where V_P and V_S are longitudinal and shear sound velocities, respectively. Φ can be also expressed by $\Phi = dP/d\rho$, with ρ as the density. From this expression and according to the Percus-Yevick equation for hard spheres [21], the seismic parameter is found to be proportional to temperature and a function of the packing fraction: $\Phi \sim Tf(\eta)$, where $f(\eta) = (1 + 2\eta)^2/(1 - \eta)^4$. Because the Φ profile in the outer core is generally considered to be parallel to that of liquid iron based on mean-atomic-weight systematics [28], it is thus possible for liquid iron data to be applied to estimate thermal structure in the outer core from the seismic parameters obtained from global seismic observation. Also required for such estimation is the temperature dependence of the packing fraction η, which is only available at ambient pressure [18]. Further experiments are needed to determine the temperature dependence of η at high pressures. From this

study, the packing fraction along the melting curve is found to be nearly constant, implying that Φ along the melting curve has a simple linear relationship with the melting temperature.

Besides the structural data for liquid iron, our study also provides experimental constraints on high pressure melting of iron. At each pressure, we monitored the structure of iron on increasing temperature. The change in x-ray diffraction/scattering from crystalline to liquid phases provides an unambiguous melting criterion, as demonstrated in Fig. 2. Defining the onset of melting in laser heated DAC has been a long-standing debate. The method in this study introduces an objective melting criterion, as compared to the visual observations widely used. In the covered pressure range, our data on melting temperatures are consistent with previous studies using visual observations [29] and x-ray diffraction with the energy dispersive technique [12], within experimental uncertainties. At the highest pressure of this study, the solid phase before melting was found to be γ-Fe, indicating that the previously determined γ-ε-1 triple point (60 ± 5 GPa, 2800 ± 200 K) [12] should be shifted to higher pressures. It needs to be noted that the present data reflect the melting of γ-Fe (Fig. 2). The melting of ε-Fe remains to be determined using the x-ray criterion.

In summary, we have measured the structure factors of liquid iron at pressures up to 58 GPa and temperatures up to 2900 K using *in situ* x-ray scattering in a laser heated diamond anvil cell. The pressure range covers the entire pressure conditions of the Martian core and is almost halfway to Earth's outer core conditions. It is found that the structure factor preserves essentially the same shape along the melting curve. Our data support the view that the viscosity of liquid iron does not change significantly along the melting curve and is close to the value at ambient pressure. In addition, our study provides experimental constraints on high pressure melting of γ-Fe to 58 GPa. The change in x-ray diffraction/scattering from crystalline to liquid phases provides an unambiguous melting criterion. Further experiments are needed to determine the melting curve of ε-Fe with the x-ray method and to study the structure of liquid iron by extending pressures to Earth's core conditions (> 135 GPa) for understanding numerous macroscopic properties, such as viscosity, self-diffusion, and electrical conductivity.

We thank Keith Brister for help during experiments. Comments by anonymous reviewers improved the manuscript. This work is supported by NSF-EAR Grant No. 0229987. The GSECARS sector is supported by the NSF (Earth Sciences Instrumentation and Facilities Program) and DOE (Geoscience Program).

*Corresponding author: shen@cars.uchicago.edu

[1] R. J. Hemley and H. K. Mao, Int. Geol. Rev. **43**, 1 (2001).
[2] C. Sanloup *et al.*, Europhys. Lett. **52**, 151 (2000).
[3] Y. Waseda and K. Suzuki, Phys. Status Solidi **39**, 669 (1970); Y. Waseda and M. Ohtani, Phys. Status Solidi (b) **62**, 535 (1974).
[4] C. F. Yoder *et al.*, Science **300**, 299 (2003).
[5] Bruce A. Buffett, Science **288**, 2007 (2000).
[6] L. Vocadlo *et al.*, Faraday Discuss. **106**, 205 (1997); A. Laio *et al.*, Science **287**, 1027 (2000); A. B. Belonoshko, R. Ahuja, and B. Johansson, Phys. Rev. Lett. **84**, 3638 (2000).
[7] C. Hausleitner and J. Hafner, J. Phys. Condens. Matter **1**, 5243 (1989).
[8] D. Alfe, G. Kresse, and M. J. Gillan, Phys. Rev. B **61**, 132 (2000).
[9] D. Alfe, G. D. Price, and M. J. Gillan, Phys. Rev. B **65**, 165118 (2002).
[10] Guoyin Shen *et al.*, Rev. Sci. Instrum. **72**, 1273 (2001).
[11] R. Boehler, M. Ross, and D. B. Boercker, Phys. Rev. Lett. **78**, 4589 (1997).
[12] Guoyin Shen *et al.*, Geophys. Res. Lett. **25**, 373 (1998).
[13] N. Sata *et al.*, Phys. Rev. B **65**, 104114 (2002).
[14] D. J. Heinz, Geophys. Res. Lett. **17**, 1161 (1990); G. Fiquet *et al.*, Phys. Earth Planet. Inter. **95**, 1 (1996).
[15] A. Kavner and T. S. Duffy, J. Appl. Phys. **89**, 1907 (2001).
[16] S. H. Shim, T. S. Duffy, and Guoyin Shen, J. Geophys. Res. **105**, 25955 (2000).
[17] J. H. Eggert *et al.*, Phys. Rev. B **65**, 174105 (2002).
[18] Yoshio Waseda, *The Structure of Non-Crystalline Materials* (McGraw-Hill, New York, 1980).
[19] G. Shen *et al.*, Rev. Sci. Instrum. **74**, 3021 (2003).
[20] N.W. Ashcroft and J. Lekner, Phys. Rev. **145**, 83 (1965).
[21] J. A. Barker and D. Henderson, Rev. Mod. Phys. **48**, 587 (1976).
[22] N. Funamori and K. Tsuji, Phys. Rev. Lett. **88**, 255508 (2002); C. Meade, R. J. Hemley, and H. K. Mao, Phys. Rev. Lett. **69**, 1387 (1992).
[23] Y. Katayama *et al.*, Nature (London) **403**, 170 (2000); W. A. Crichton *et al.*, Nature (London) **414**, 622 (2001).
[24] M. D. Rutter *et al.*, Phys. Rev. B **66**, 060102 (2002); David P. Dobson, Phys. Earth Planet. Inter. **130**, 271 (2002).
[25] V.V. Brazhkin and A. G. Lyapin, Phys. Usp. **43**, 493 (2000).
[26] D. J. Stevenson, Phys. Earth Planet. Inter. **22**, 42 (1980); D. J. Stevenson, Science **214**, 611 (1981).
[27] O. L. Anderson and D. G. Isaak, Am. Mineral. **85**, 376 (2000).
[28] J. M. Brown and R. G. McQueen, J. Geophys. Res. **91**, 7485 (1986).
[29] G. Shen, P. Lazor, and S. K. Saxena, Phys. Chem. Miner. **20**, 91 (1993); R. Boehler, Nature (London) **363**, 534 (1993); S. K. Saxena, G. Shen, and P. Lazor, Science **264**, 405 (1994).